Spectroscopic Determination of Electron and Hole Effective Masses in a Nanocrystalline Semiconductor Film

Brendan Enright and Donald Fitzmaurice*

Department of Chemistry, University College, Dublin 4, Ireland

Received: April 24, 1995; In Final Form: October 16, 1995[⊗]

Spectroelectrochemical techniques may be used to determine the absolute energy of the valence and conduction band edges of a transparent nanocrystalline semiconductor electrode. Such determinations have been made for ZnO (wurtzite) and TiO_2 (anatase) electrodes constituted from nanocrystallites possessing average radii close to, and substantially larger than, the radius of a bound exciton in the corresponding bulk semiconductor. Electrodes constituted from crystallites whose radii are close to that of a bound exciton exhibit an onset for band gap absorption that is significantly blue-shifted. Those constituted from crystallites whose radii are substantially larger than that of a bound exciton exhibit an absorption onset characteristic of the bulk material. Knowing the absolute energies of band edges, the observed increase in band gap energy for electrodes constituted from confined nanocrystallites may be partitioned between the conduction and valence bands. A subsequent analysis permits determination of the effective electron and hole mass in a nanocrystalline film. Most notably, it has proved possible to determine, for the first time, a value for the effective hole mass in TiO_2 (anatase) of $(0.8 \pm 0.2)m_e$.

Introduction

Transparent nanocrystalline semiconductor electrodes have been the subject of numerous recent investigations.[1,2] This increased interest can largely be attributed to the development of efficient regenerative photoelectrochemical cells based on dye sensitized nanocrystalline semiconductor electrodes.[3] Of particular interest is the mechanism by which photoinjected electrons are transported to the external circuit.[2] It is in this context that we describe a new spectroelectrochemical technique that may be used to determine the effective mass of a charge carrier in a nanocrystalline semiconductor film. Subsequent calculation of carrier mobilities and diffusion coefficients is possible. The approach adopted is outlined below.

Spectroelectrochemical measurements are used to determine the potential energy of the conduction band edge (V_{cb}) of a transparent nanocrystalline semiconductor electrode at the semiconductor−liquid electrolyte interface (SLI).[1] Specifically, V_{cb} has been determined for ZnO (wurtzite) and TiO_2 (anatase) electrodes constituted from nanocrystallites possessing radii substantially larger than that of a bound exciton in the corresponding bulk semiconductor.[1a] Such electrodes do not, as expected, exhibit optical confinement effects, and a band gap energy (E_g) characteristic of the bulk material is measured.[4] With knowledge of E_g and V_{cb}, the potential of the valence band edge (V_{vb}) at the SLI may be deduced. Similar experiments for ZnO and TiO_2 electrodes constituted from nanocrystallites possessing radii close to that of a bound exciton in the bulk semiconductor were also performed.[1a,5] Such electrodes do exhibit optical confinement effects, E_g being significantly larger than that measured for the bulk semiconductor. From knowledge V_{cb} and E_g, as above, V_{vb} may be deduced.

Measurements, such as those outlined above, allow quantitative partition of the increase in E_g due to confinement effects between the conduction and valence bands. A subsequent analysis of these data permits determination of the effective electron (m_e*) and hole (m_h*) masses. These values are compared, where available, with previously determined values for single crystal and polycrystalline ZnO and TiO_2 electrodes. In addition, mobilities and diffusion coefficients for carriers within the constituent crystallites of the above electrodes are calculated.

Finally, we have adopted the notation V_{cb} and refer to the potential of the conduction band edge at the SLI. In previous reports the quantity V_{cb} has been termed the flat band potential and denoted V_{fb}.[1a−c] Similarly, we refer to the potential of the valence band edge at the SLI, denoted V_{vb}. This notational change recognizes that for nanocrystalline semiconductor electrodes use of the term flat band potential is not entirely appropriate. Specifically, it appears that band bending and an associated space charge layer are absent under classical *depletion* conditions.[3f] That is, the space charge layer capacitance (C_{SC}) may be taken as zero at applied potentials more positive than V_{cb}. However, it appears that band bending and an associated space charge layer are present under classical *accumulation* conditions.[3f] That is, C_{SC} may be taken as nonzero at applied potentials more negative than V_{cb}. As discussed below, direct determination of C_{SC} for nanocrystalline electrodes currently presents experimental difficulties, although calculation of accurate values is possible.[1a,b] Concerning the Helmholtz capacitance (C_H), values determined for the bulk material under similar conditions may justifiably be used.[1a,b] Importantly, we note that the absence of band bending at positive applied potentials does not affect the validity of the models underlying data analysis for determination of V_{cb}, these models being based on occupation of available states in the conduction band at negative applied potentials.

Experimental Section

I. Preparation of Transparent Nanocrystalline ZnO Electrodes. Ethanolic dispersions of ZnO were prepared at 0 °C following the method of Spanhel and Anderson and concentrated to 140 g/L.[6] Concentrated dispersions were used to form a ZnO film on fluorine doped SnO_2 conducting glass supplied by Glastron. Drying in air at room temperature for 1 h gave rise to a nanocrystalline ZnO film in ohmic contact with

* Author to whom correspondence should be addressed.
[⊗] Abstract published in *Advance ACS Abstracts,* December 15, 1995.

0022-3654/96/20100-1027$12.00/0 © 1996 American Chemical Society

the conducting glass substrate. Electrodes prepared as described above exhibit quantum confinement effects and are referred to as *confined electrodes*. Electrodes prepared using a ZnO dispersion previously aged at room temperature exhibit no confinement effects and are referred to as *bulk electrodes*.[1a]

II. Preparation of Transparent Electrodeposited TiO_2 Electrodes. Nanocrystalline TiO_2 electrodes were prepared, following the method of Kavan *et al.*, by oxidative hydrolysis of $TiCl_3$ on fluorine doped SnO_2 conducting glass supplied by Glastron.[5] Briefly, a 0.05 mol dm^{-3} solution of $TiCl_3$ was prepared using distilled−deionized water deaerated with argon and adjusted to pH 3 using a 10% deaerated solution of $NaHCO_3$. Electrodeposition was carried out at 0.00 V (SCE) during 4 h in an electrochemical cell.

III. Potential Dependent Spectroscopy. Nanocrystalline TiO_2 and ZnO electrodes, prepared as described above, formed the working electrodes of a closed three-electrode single compartment electrochemical cell, the counter electrode being platinum and the reference electrode, a saturated calomel electrode (SCE). The electrolyte solution, prepared using distilled−deionized water, was 0.2 mol dm^{-3} $LiClO_4$. pH was adjusted using $HClO_4$ and KOH. Potential control was provided by a Thompson Ministat precision potentiostat connected to a Thompson Electrochem Miniscan potential sweep generator. The above cell was incorporated into the sample compartment of a Hewlett-Packard 8452A diode array spectrophotometer. For each determination of V_{cb} a new working electrode and freshly prepared electrolyte solution were used. All potentials are reported against SCE.

IV. Characterization Techniques. Transmission electron micrographs (TEMs) and scanning electron micrographs (SEMs) were obtained using a JEOL 2000FX TEMSCAN. X-ray diffractometry (XRD) was performed using a Phillips PW system.

Results

I. Spectroscopy of Nanocrystalline ZnO Films. ZnO crystallites formed at 0 °C have an average diameter of 4.0 ± 0.2 nm as determined by TEM; see Figure 1a. Confirmation of domain size by XRD was not possible. The onset for optical absorption is significantly blue-shifted to 350 nm at 300 K. Dispersions aged at room temperature for 120 h have an average crystallite diameter of 12.0 ± 0.2 nm as determined by TEM; see Figure 1a. XRD confirms wurtzite structure and suggests a domain size of 13 nm. Crystallite growth is accompanied by a red shift in the onset for optical absorption to 380 nm at 300 K. UV/vis spectroscopy of electrodes formed by deposition of ZnO crystallites is similar to that observed for the corresponding ethanolic dispersions. Specifically, electrodes prepared from freshly prepared dispersions possess a blue-shifted spectrum, while those formed from aged dispersions possess a bulk spectrum; see Figure 1b.

II. Potential Dependent Spectroscopy of Nanocrystalline ZnO Films. The absorbance spectrum at 0.00 V of a confined ZnO electrode was recorded. Difference spectra were subsequently measured as a function of applied potential. At negative potentials an absorbance loss, assigned to accumulation of electrons in the conduction band of ZnO, is observed at wavelengths shorter than 350 nm.[1a] As expected, this Burstein shift is observed at increasingly negative potentials for higher pHs.[7] No absorbance that may be assigned to free conduction band electrons or electrons localized at bulk or surface defects is observed in the 350−800 nm region. Experiments were also performed using bulk ZnO electrodes. The results of these experiments are qualitatively similar to those obtained using confined electrodes, although the Burstein shift is observed at wavelengths shorter than about 380 nm. The results of experiments at pH 12.0 for confined and bulk electrodes are shown in Figure 2.

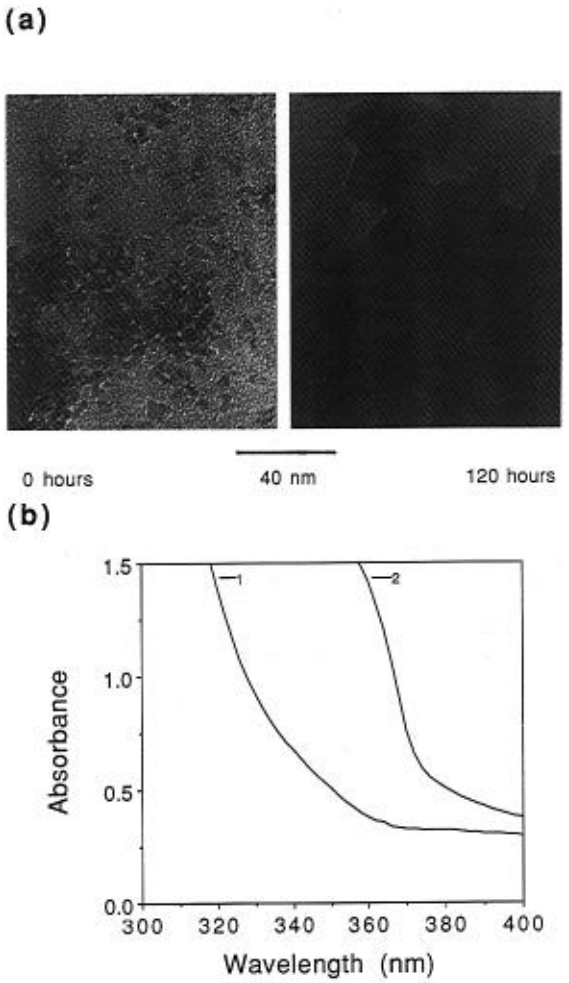

Figure 1. (a) Transmission electron micrographs of crystallites constituting freshly prepared ZnO dispersion (0 h, average diameter 4 nm) and the crystallites constituting the same dispersion aged at room temperature (120 h, average diameter 12 nm). (b) Absorbance spectrum of ZnO electrodes prepared from (1) freshly prepared and (2) aged ZnO dispersions in a.

III. Determination of V_{cb} for Nanocrystalline ZnO Films. As a consequence of there being no measurable free electron absorbance by ZnO, data such as that in Figure 2 may be analyzed to obtain a value for V_{cb}.[1a] Specifically, the relationship between the magnitude of a dynamic Burstein shift (ΔE) and the number of electrons present in the available states of the conduction band is given by eq 1, where E_f is the Fermi

$$\Delta E = \left(1 + \frac{m_e^*}{m_h^*}\right)[E_f - E_{cb} - 4k_BT] \qquad (1)$$

level. E_{cb}, the energy of the conduction band edge at the SLI, is approximated by eq 2. In eq 1 the quantity $4k_BT$ accounts

$$E_f - E_{cb} = \frac{h^2}{2m_e^*}\left(\frac{3n_{cb}}{8\pi}\right)^{2/3} \qquad (2)$$

for thermal excitation of electrons accumulated in the conduction band from states whose energies are less than E_f to states whose energies lie above E_f. In experiments for which results are reported accumulation of electrons in the conduction band is potentiostatically controlled. Consequently, it is assumed that

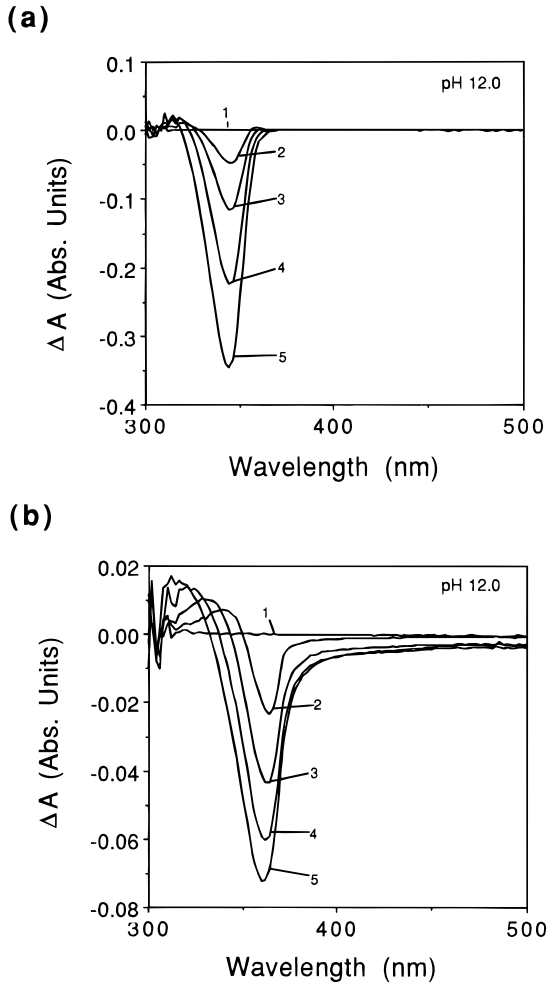

Figure 2. (a) Difference absorbance spectra at pH 12.0 of confined ZnO electrode measured at the following applied potentials (V, SCE): (1) 0.00, (2) −1.20, (3) −1.25, (4) −1.30, and (5) −1.35 V. (b) Difference absorbance spectra at pH 12.0 of bulk ZnO electrode measured at the following applied potentials (V, SCE): (1) 0.00, (2) −1.00, (3) −1.10, (4) −1.20, and (5) −1.30 V.

all states which lie below E_f are filled, that all states which lie above are vacant, and that ΔE is given by eq 3. We can write

$$\Delta E = \left(1 + \frac{m_e^*}{m_h^*}\right)[E_f - E_{cb}] \qquad (3)$$

eq 3 in terms of electrochemical potentials to yield eq 4, where

$$\Delta E = -e_0\left(1 + \frac{m_e^*}{m_h^*}\right)(V_f - V_{cb}) \qquad (4)$$

$e_o = 1.602 \times 10^{-19}$ J/eV. We assume the Fermi level in the semiconductor electrode is at the same energy as the Fermi level in the conducting glass substrate. From experiment the potential difference between the Fermi level in the bulk semiconductor and the potential of the bulk electrolyte solution, i.e., $(V_f - V_{bulk})$, is known. However, ΔE depends on the potential drop across the semiconductor electrode, i.e., on $(V_f - V_{cb})$. We relate $(V_f - V_{bulk})$ to $(V_f - V_{cb})$ by taking into account C_{SC} and C_H. This, as discussed above, is appropriate at applied potentials more negative than V_{cb} since the width of the associated space charge layer is commensurate with the diameter of the constituent crystallites of the semiconductor film.[1b,3f] We note, also as discussed above, that a similar treatment at applied potentials more positive than V_{cb} could not be justified.

The question arises as to how to quantify C_{SC} and C_H at negative applied potentials for a nanocrystalline semiconductor electrode. Concerning C_{SC}, direct measurement of this quantity using Mott−Schottky techniques has proved problematic.[1c] Therefore this quantity has been calculated as described in detail elsewhere.[1a] Briefly, however, the rate of change of the excess charge with applied potential is calculated and is equated to C_{SC}. Concerning C_H, relevant values determined for the bulk semiconductor in contact with an electrolyte solution are used.[1a,1c] It is further assumed that C_H is independent of the applied potential. We note, in each case the capacitances are in units of F m^{-2}; i.e., the actual surface area, and therefore the surface roughness of the nanocrystalline electrode, is accounted for. As these capacitances are in series, eq 5 relates $(V_f - V_{bulk})$

$$(V_f - V_{cb}) = \left(\frac{C_H}{C_{SC} + C_H}\right)(V_f - V_{bulk}) \qquad (5)$$

to $(V_f - V_{cb})$. The correction to the measured quantity $(V_f - V_{bulk})$ is calculated individually for each potential, C_{SC} being a function of $(V_f - V_{cb})$. The relationship between C_{SC} and $(V_f - V_{cb})$ has been discussed in detail elsewhere.[1b] C_{SC} was calculated to be between 0.006 and 0.007 F m^{-2} at all applied potentials for which data are reported. The value for C_H used was 0.85 F m^{-2}.[8] It is assumed that the potential drop through the electrolyte solution can be neglected as a consequence of the cell geometry. The intrinsic carrier concentration was taken as 10^{24} m^{-3}. This represents the lower end of the range of reported values for polycrystalline ZnO electrodes (10^{23}−10^{26} m^{-3}).[9] The lower end of the available range, being chosen to account for the known effect of Li^+ atoms, is expected to be present in the ZnO crystallites.[10] The Burstein shift can be estimated from the bleach width at half amplitude of the data shown in Figure 2. Plotting the Burstein shift ($\Delta E/e_0$) against $(V_f - V_{cb})$ results in a straight line relationship; see Figure 3. The intercept of such a plot with the axis represents the value of $(V_f - V_{cb})$ for which the Burstein shift is zero; i.e., $V_f = V_{cb}$.

The average of the results of *five* such analyses for confined and bulk nanocrystalline ZnO electrodes at pH 3.0 and pH 12.0 are given in Table 1. From the change in V_{cb} and E_g, it is possible to deduce the change in V_{vb}. It is apparent that at pH 3.0, about two-thirds of the energy of confinement is accounted for by an increase in energy of the available states of the valence band. The remaining third is manifest in an increase in the energy of the available states of the conduction band. The results obtained at pH 12.0 are discussed below.

IV. Spectroscopy of Nanocrystalline TiO_2 Films. SEM and XRD studies have shown that an initially deposited TiO_2 electrode consists of an 8 μm thick nanoporous layer of amorphous 2.0 ± 0.2 nm particles.[5,11] The observed blue shift in the absorption onset to 345 nm at 300 K is a consequence of confinement of photogenerated electron−hole pairs within the constituent particles of the TiO_2 electrode. Annealing the above electrode in air at 450 °C for 24 h results in a 25% weight loss and yields a broadened XRD spectrum for anatase. The observed weight loss is attributed to evolution of H_2O from surface OH groups and is accompanied by a 30% reduction in electrode thickness. The observed broadening in the XRD spectrum suggests a domain size of 8.0 ± 0.2 nm. The latter being consistent with the observed red-shift of the absorption onset to the bulk value of 380 nm at 300 K expected for particles having a diameter greater than 7 nm.[12] The UV/vis and XRD spectra referred to above are shown in Figure 4.

V. Potential Dependent Spectroscopy of Nanocrystalline TiO_2 Films. The absorbance spectrum at 0.00 V of a confined

TABLE 1: Potential of Conduction Band Edge at the SLI for Bulk and Confined Nanocrystalline ZnO Electrodes in Water Containing 0.2 mol dm^{-3} $LiClO_4$

V_{cb} bulk ZnO[a,b] (V, SCE)		V_{cb} confined ZnO[a,c] (V, SCE)		
pH 3.0	pH 12.0	pH 3.0	pH 12.0	ΔE_g (V)
-0.22 ± 0.02 [d]	-0.66 ± 0.03 [d]	-0.42 ± 0.02 [d]	-0.93 ± 0.02 [d]	0.27 ± 0.01[d]

[a] All potentials are versus SCE. [b] The average diameter of nanocrystallites constituting the bulk ZnO film is 12.0 ± 0.2 nm. [c] The average diameter of nanocrystallites constituting the confined ZnO film is 4.0 ± 0.2 nm. [d] Values are the average of five individual determinations.

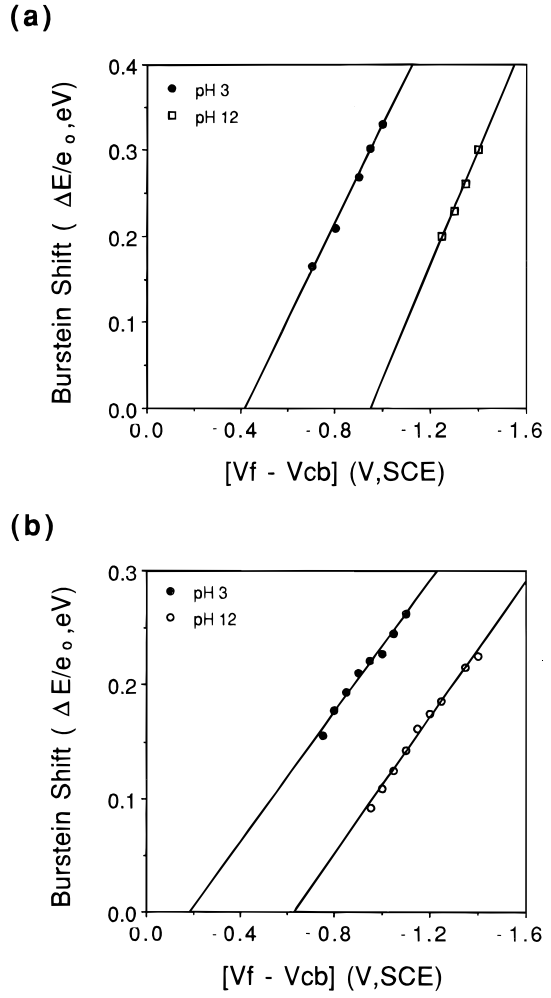

Figure 3. (a) Plot of the Burstein shift ($\Delta E/e_0$, eV) against the applied potential ($V_f - V_{cb}$, SCE) for a confined ZnO electrode at pH 3.0 and pH 12.0. (b) Plot of the Burstein shift ($\Delta E/e_0$, eV) against the applied potential ($V_f - V_{cb}$, SCE) for a bulk ZnO electrode at pH 3.0 and pH 12.0.

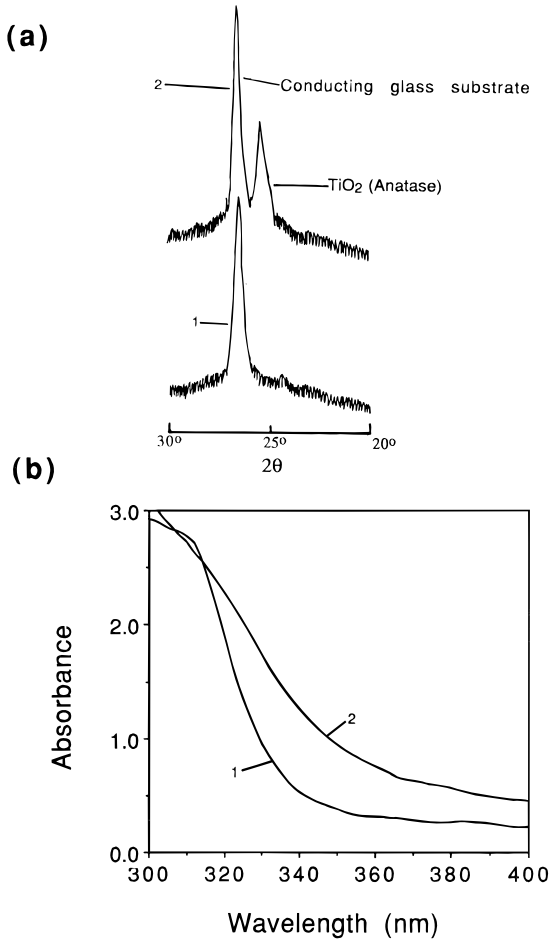

Figure 4. (a) X-ray diffraction spectrographs (1) of initially deposited TiO_2 electrode and (2) following firing at 450 °C in air for 24 h. (b) Absorbance spectrum of (1) of initially deposited TiO_2 electrode and (2) following firing at 450 °C in air for 24 h.

TiO_2 electrode was recorded. Difference spectra were subsequently measured as a function of applied potential. At negative potentials an absorbance loss, assigned to accumulation of electrons in the TiO_2 conduction band, is observed at wavelengths shorter than 345 nm.[1b] At wavelengths longer than 345 nm, an absorbance assigned to free conduction band electrons and electrons localized at bulk or surface defects is observed.[1b] The above absorbance changes are observed at more negative potentials for higher pHs.[13] Experiments using TiO_2 electrodes fired in air at 450 °C for 24 h were also performed. The results of these experiments are qualitatively similar to those obtained using confined electrodes, although the Burstein shift is observed at wavelengths shorter than about 380 nm. The results of experiments at pH 11.0 for confined and bulk electrodes are shown in Figure 5.

VI. Determination of V_{cb} for Nanocrystalline TiO_2 Films. Absorbance at 780 nm, assigned principally to free conduction band electrons, was measured as a function of applied potential for initially deposited electrodes at pH 2.0 and pH 11.0; see Figure 6. Similar measurements were made using electrodes annealed in air at 450 °C for 24 h; see Figure 6b. Kavan *et al.* have shown that E_{cb} for electrodeposited TiO_2 electrodes fired in argon at 450 °C for 1 h is given by eq 6.[5] Therefore, V_{cb} is

$$V_{cb} = -0.25 - (0.06\text{pH}) \text{ [V, SCE]} \quad (6)$$

taken as -0.37 and -0.91 V at pH 2.0 and 11.0, respectively, for the annealed TiO_2 electrodes. V_{cb} for confined TiO_2 electrodes may therefore be determined from the measured shift in the onset for absorbance at 780 nm following annealing. Also known from measurement of the corresponding UV/vis absorbance spectra is the change in E_g upon annealing.

The average of the results of *five* such analyses for confined and bulk nanocrystalline TiO_2 electrodes at pH 2.0 and pH 11.0 are given in Table 2. From the change in E_{cb} and E_g, it is possible to deduce the change in V_{vb}. It is apparent that at pH 2.0 and pH 11.0, virtually all the energy of confinement is accounted for by an increase in energy of the available states

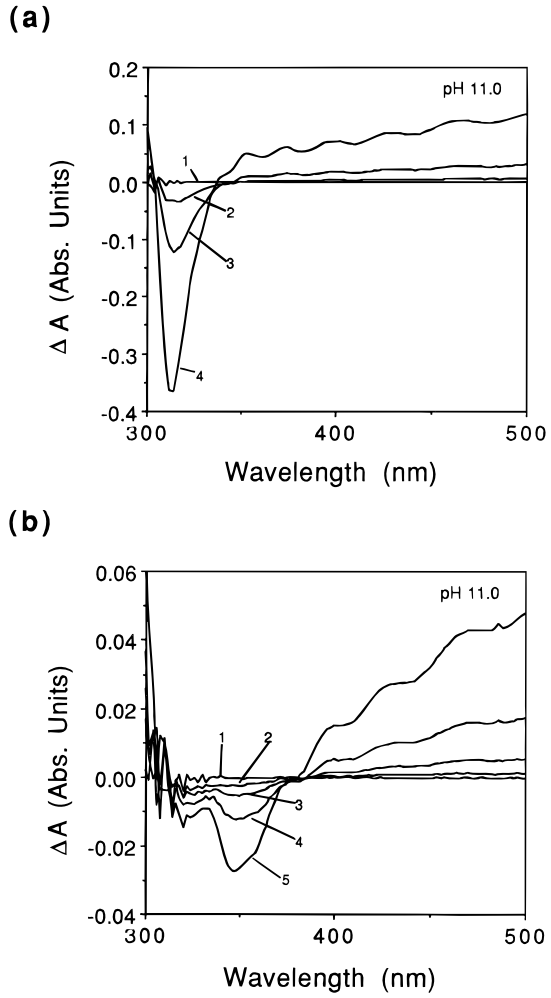

Figure 5. (a) Difference absorbance spectra at pH 11.0 of confined TiO_2 electrode measured at the following applied potentials (V, SCE): (1) 0.00, (2) −1.20, (3) −1.30, and (4) −1.40 V. (b) Difference absorbance spectra at pH 11.0 of bulk TiO_2 electrode measured at the following applied potentials (V, SCE): (1) 0.00, (2) −1.10, (3) −1.20, (4) −1.30, and (5) −1.40 V.

TABLE 2: Potential of Conduction Band Edge at the SLI for Bulk and Confined Nanocrystalline TiO_2 Electrodes in Water Containing 0.2 mol dm^{-3} $LiClO_4$

V_{cb} bulk TiO_2[a] (V, SCE)		V_{cb} confined TiO_2[a] (V, SCE)		
pH 2.0	pH 11.0	pH 2.0	pH 11.0	ΔE_g (V)
−0.37 [d]	−0.91 [d]	−0.35 ± 0.02 [e]	−0.91 ± 0.01 [e]	0.33 ± 0.01 [e]

[a] All potentials are versus SCE. [b] The average diameter of nanocrystallites constituting the bulk TiO_2 film is 8.0 ± 0.2 nm. [c] The average diameter of nanocrystallites constituting the confined TiO_2 film is 2.0 ± 0.2 nm. [d] V_{cb} for bulk TiO_2 films from eq 6. [e] Values are the average of five individual determinations.

of the valence band. No significant increase in the energy of the available states of the conduction band is observed.

Discussion

I. Determination of Effective Electron and Hole Masses in ZnO. The band structure of ZnO (hexagonal wurtzite) has been studied extensively. The absorption onset of this semiconductor corresponds to a direct transition between parabolic bands at the band gap energy of 3.2 eV (300 K).[10] The predicted relationship between the absorption coefficient (α) and the energy of the exciting photon ($h\nu$) for a direct transition semiconductor is given by eq 7.[14] The coefficient A has been

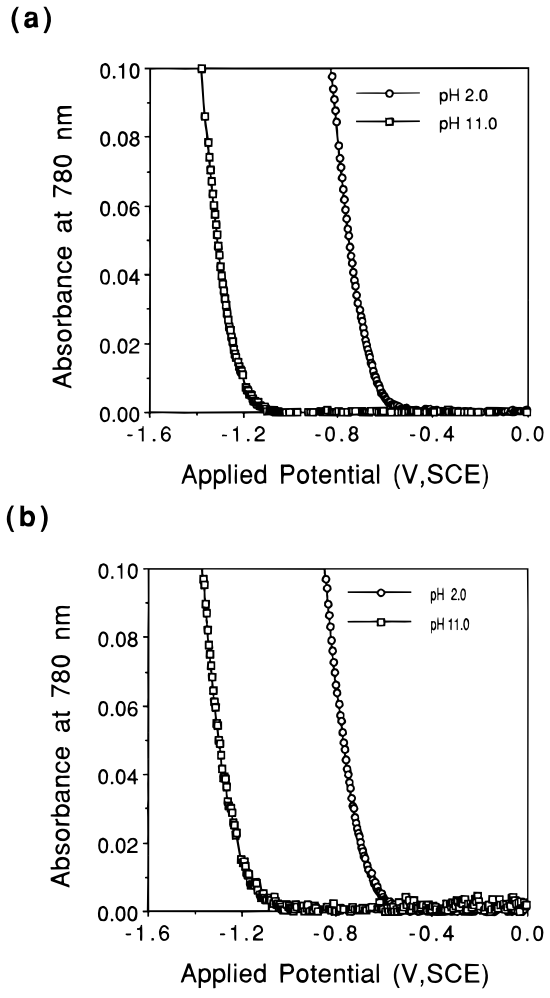

Figure 6. (a) Absorbance at 780 nm of an electrodeposited TiO_2 electrode prior to firing, plotted against applied potential at pH 2.0 and pH 11.0. (b) Absorbance at 780 nm of electrode in a following firing in air at 450 °C for 24 h plotted against applied potential at pH 2.0 and pH 11.0.

$$\alpha(h\nu) = A[h\nu - E_g]^{1/2} \qquad h\nu > E_g \tag{7}$$

derived by Bardeen *et al.*[15] Equation 7 predicts a steeply rising absorption edge at photon energies greater than E_g and no absorption at photon energies below E_g. In practice, α increases exponentially from energies significantly below E_g. The observed exponential dependence of α at energies below E_g often obeys Urbach's rule, given by eq 8, where σ is a constant.[16]

$$\alpha(h\nu) = \alpha(E_g)\exp\left[\frac{\sigma}{kT}(h\nu - E_g)\right] \qquad h\nu < E_g \tag{8}$$

It is suggested this phenomenon has its origin in the existence of sub-band-gap phonon assisted transitions.[17] At low temperature, a series of resolved peaks are observed in the ZnO absorption edge.[18] These absorption features are assigned to discrete states of a Wannier exciton.[19−22] A general theory of exciton absorption in media of high dielectric coefficient, where electron−hole interaction is weak, was developed by Elliott based on an effective mass approximation.[23] The Bohr radius, r_B, of the first excitonic state ($n = 1$) is given by eq 9. The

$$r_B = \frac{\epsilon h^2}{\mu_{eff}\pi e^2} \tag{9}$$

corresponding binding energy E_B ($n = 1$) is given by eq 10,

$$E_B = \mu_{eff} e^4/8\epsilon^2 h^2 \tag{10}$$

where $\epsilon = \epsilon_r\epsilon_0$ (ϵ_r being the dielectric coefficient at optical frequencies) and μ_{eff} is the reduced effective mass of the electron−hole pair given by eq 11. These exciton transitions

$$\mu_{eff} = \frac{m_e{}^* m_h{}^*}{m_e{}^* + m_h{}^*} \tag{11}$$

will be found at energies given by eq 12. The Bohr radius of

$$E_{ex} = E_g - E_B \tag{12}$$

the lowest-energy exciton in bulk ZnO ($n = 1$) is calculated to be 1.3 nm using eq 9 and values for $m_e{}^* = 0.24m_e$, $m_h{}^* = 0.45m_e$, and $\epsilon_r = 3.7$.[4] The corresponding binding energy is 0.156 eV ($n = 1$).

In a spherical crystallite of ZnO whose radii, R, approachs that of the Bohr radius, we expect to observe confinement effects. Specifically, the electron−hole pair formed, following absorption of a photon more energetic than E_g, is spatially confined in a three-dimensional spherical potential well. The electron−hole pair does not form an exciton, i.e., an electron and hole bound by mutual interactions and able to thermally dissociate into free carriers. Nevertheless, the electron and hole do give rise to discrete exciton-like states. Following the treatment of Brus, it is possible to estimate energies for the single electron and single hole MOs associated with such states using eqs 13a and 13b.[24] The coefficients ϕ_{nl} are tabulated by Flugge.[25]

$$E_{nl}^{cb}(R) = E_{cb} + \frac{h^2}{2\pi^2 m_e{}^* R^2}\phi_{nl} \tag{13a}$$

$$E_{nl}^{vb}(R) = E_{vb} + \frac{h^2}{2\pi^2 m_h{}^* R^2}\phi_{nl} \tag{13b}$$

In the analysis outlined above, it is assumed that electron and hole motions are uncorrelated. In practice, this motion is correlated through a shielded Coulomb interaction. Consequently the energy of the lowest energy transition in a spherical crystallite is given by eq 14.[4,24] It is useful to rewrite eq 14 in

$$E(R) = E_g + \frac{h^2}{8R^2}\left[\frac{1}{m_e{}^*} + \frac{1}{m_h{}^*}\right] - \frac{1.8e^2}{4\pi\epsilon_0\epsilon_r R} \tag{14}$$

terms of the contribution of the increase in energy of the lowest conduction band state and the lowest valence band state (eqs 15a−c). $m_e{}^*$, $m_h{}^*$, and ϵ_r may be determined directly from the

$$E_{opt} = E_g + \Delta E_{cb} + \Delta E_{vb} \tag{15a}$$

$$\Delta E_{cb} = \frac{h^2}{8m_e{}^* R^2} - \frac{0.9e^2}{4\pi\epsilon_0\epsilon_r R} \tag{15b}$$

$$\Delta E_{vb} = \frac{h^2}{8m_h{}^* R^2} - \frac{0.9e^2}{4\pi\epsilon_0\epsilon_r R} \tag{15c}$$

data in Table 1. Specifically, rearrangement of eq 15b gives eq 16. The points in a plot of ($\Delta E_{cb}R$) against ($1/R$) are

$$\Delta E_{cb}R = \frac{h^2}{8m_e{}^*}\left(\frac{1}{R}\right) - \frac{0.9e^2}{4\pi\epsilon_0\epsilon_r} \tag{16}$$

connected by a straight line whose slope and intercept are

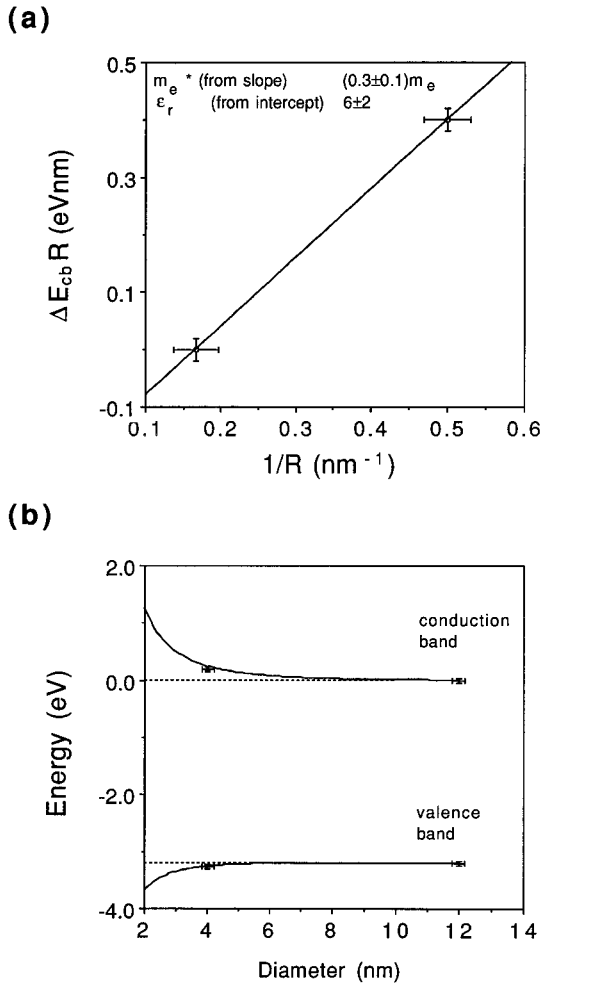

Figure 7. (a) $\Delta E_{cb}R$ plotted against $1/R$ for ZnO (data taken from Table 1). (b) Using values determined for $m_e{}^*$, $m_h{}^*$, and ϵ_r as shown in a, E_g, predicted using eq 15 as a function of particle radius. Also plotted are the experimentally determined changes in the energy of the valence and conduction band edges.

equated to ($h^2/8m_e{}^*$) and ($-0.9e^2/4\pi\epsilon_0\epsilon_r$), respectively; see Figure 7a. The resulting values for $m_e{}^*$ and ϵ_r, being ($0.3 \pm 0.1)m_e$ and 6 ± 2, respectively, are in good agreement with those reported for the bulk semiconductor.[4,14,24] A similar analysis yields eq 17, from which values for $m_h{}^*$ of (0.8 ± 0.5)-

$$\Delta E_{vb}R = \frac{h^2}{8m_h{}^*}\left(\frac{1}{R}\right) - \frac{0.9e^2}{4\pi\epsilon_0\epsilon_r} \tag{17}$$

m_e are determined. As for the electron, the effective hole mass agrees well with that reported for the bulk semiconductor.[4,14,24] Using eqs 15b and 15c, it is possible to predict the increase in energy of the conduction and valence bands states as a function of crystallite diameter; see Figure 7b. These calculations were made using the values for $m_e{}^*$ ($0.3m_e$), $m_h{}^*$ ($0.8m_e$), and ϵ_r (6) determined as described above. The measured changes in the energy of the lowest states in the conduction and valence bands for 4 and 12 nm diameter particles are also plotted in Figure 7b.

The analysis applied above assumes a direct transition between parabolic bands and effective masses which are isotropic. These assumptions are appropriate to bulk ZnO.[10,26] The resulting values for $m_e{}^*$, $m_h{}^*$, and ϵ_r agree with those measured at optical frequencies for the bulk semiconductor, although determined for a nanocrystalline film.[4,14,24] This agreement is attributed to the fact that experiments were

performed using films whose constituent nanocrystallites possess radii close to, but not smaller than, the Bohr radius of a bound exciton. Under these conditions, referred to as moderate confinement conditions, interaction with surface states and excitation of discrete states is less important. Further, the tendency of the effective mass approximation to overestimate the measured blue shift in the onset for band gap absorption is generally small for particles larger than the Bohr radius.[27] Finally, the observation that at pH 12.0 the change in V_{vb} accounts completely for the measured change in E_g cannot be explained at present. However, it is possible that particle dissolution or adsorption of hydroxyl groups under basic conditions is important. This view is consistent with the suggestion of Hoyer *et al.* that removal of a hydroxide appeared to be a prerequisite for development of a bulklike band structure in ZnO nanocrystallites.[1d]

II. Determination of the Effective Electron and Hole Masses in a Nanocrystalline TiO_2 Film. The band structure of the rutile form of TiO_2 has been studied extensively.[28] The two lowest energy transitions at about 3.03 and 3.19 eV are indirect.[29] The predicted relationship between the absorption coefficient (α_a) and the energy of the exciting photon ($h\nu$) for an indirect transition accompanied by absorption of a phonon of energy E_p is given by eq 18.[14] The corresponding relationship

$$\alpha_a(h\nu) = \frac{A(h\nu - E_g + E_p)^2}{\exp(E_p/kT) - 1} \qquad h\nu > E_g - E_p \qquad (18)$$

for an indirect transition accompanied by phonon emission is given by eq 19.[14] Since both phonon absorption and emission

$$\alpha_e(h\nu) = \frac{A(h\nu - E_g - E_p)^2}{1 - \exp(-(E_p/kT))} \qquad h\nu > E_g + E_p \qquad (19)$$

are possible when $h\nu > E_g + E_p$, the absorption coefficient is given by eq 20. The first direct transition is observed at about

$$\alpha(h\nu) = \alpha_a(h\nu) + \alpha_e(h\nu) \qquad (20)$$

3.45 eV, and such a transition is described by eq 7 given above.[30] No detailed information concerning the band structure of anatase in available, although a value of 3.2 eV has been reported for the band gap energy.[31]

A range of values has been reported in the literature for the effective masses of the electron in the rutile form of TiO_2. Kormann *et al.* referred to recently reported values in the range $5m_e$ to $13m_e$ and used the average of these values of $9m_e$ for calculations related to confinement effects in colloidal anatase TiO_2 particles.[12] Other workers have suggested values in the range $30m_e$ to $100m_e$.[32] Generally, the large effective mass of the electron in TiO_2 is accounted for by the d-band character of the conduction band and the consequent polaron transport mechanism. Regarding the effective mass of the hole, it appears no direct measurements have been reported. Kormann *et al.* have estimated a value of about $2m_e$ and suggest the actual value is probably less than $1m_e$.[12]

Better agreement exists concerning values for dielectric coefficient of rutile. Specifically, Grant reported a value of 173 measured parallel to the *c* axis and a value of 89 measured perpendicular to it.[33] Values obtained by Daude *et al.* of 174 and 86, respectively, are similar.[27a] In fact, of more relevance in this context is the dielectric coefficient at optical frequencies. This quantity is estimated, using the square of the visible refractive index, to be 9. Using the average values for m_e^* ($9m_e$) and m_h^* ($2m_e$) given by Kormann *et al.* and a value for ϵ_r (9) estimated from the refractive index, we obtain from eq 9 a value for r_B of about 0.3 nm. The corresponding binding energy is estimated to be 0.275 eV from eq 10.

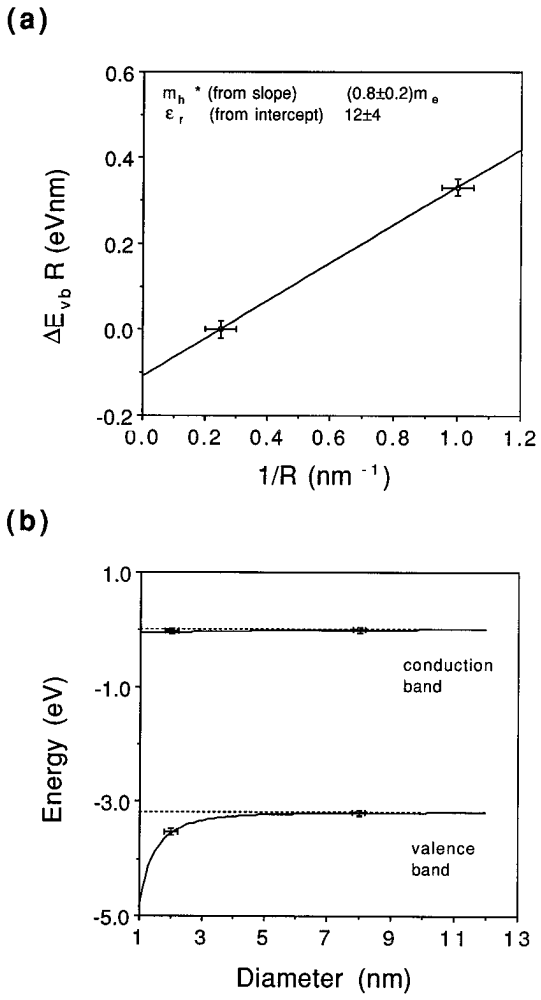

Figure 8. (a) $\Delta E_{vb}R$ plotted against $1/R$ for TiO_2 (data taken from Table 2). (b) Using values determined for m_e^*, m_h^*, and ϵ_r as shown in a, E_g predicted using eq 15 as a function of particle radius. Also plotted are the experimentally determined changes in the energy of the valence and conduction band edges.

The data presented in Table 2 are broadly consistent with the above summary. Specifically, m_e^* being between 1 and 2 orders of magnitude larger than m_h^*, it is expected that an increase in band gap energy with a decrease in average particle diameter will be manifest predominantly in an increase in the energy of the available states of the valence band. This is clearly the case with a change in E_g of 0.33 eV, resulting in no significant change in the energy of the available states of the conduction band at pH 2.0 and pH 11.0.

An analysis of the data presented in Table 2 allows a value of $(0.8 \pm 0.2)m_e$ for m_h^* to be determined; see Figure 8a. This appears to be the first experimental determination of this parameter. A value of 12 ± 4 is determined for ϵ_r. The measured change in the energy of the conduction band is not significant and prevents accurate determination of m_e^*. However, using the above values for m_h^* and ϵ_r, the measured change in E_g is consistent with a value for m_e^* of greater than $10m_e$. Taking the values for m_e^* ($10m_e$), m_h^* ($0.8m_e$), and $\epsilon_r(12)$ determined as above and using eqs 15b and 15c, we predict the size dependence for the energy of the valence and conduction bands; see Figure 8b. The measured changes in the energy of the lowest states in the valence and conduction bands for 2 and 8 nm particles are also plotted. Agreement is good.

The above analysis assumes that the effective masses and optical dielectric coefficient are isotropic. The validity of these assumptions is discussed by Brekenbridge and Hosler for rutile.[32a]

III. Some Previous Studies. The work described above represents a spectroelectrochemical method that may be used to determine the effective electron and hole masses in a transparent nanocrystalline semiconductor electrode. We compare our results with those available in the literature and consider some related work.

In the case of ZnO, accepted values for effective electron and hole masses determined at optical frequencies are $0.24m_e$ and $0.45m_e$, respectively. These are termed bare effective masses. The optical dielectric coefficient is 3.7. It is known that effective masses determined at lower frequencies are larger than those determined at optical frequencies, the former being termed the polaron effective mass. In the case of ZnO the polaron effective mass is estimated by Baer to be $0.29m_e$, the larger value being calculated on the basis of the coupling of electron motion with the highest frequency optical phonon at 590 cm^{-1}.[26] This value is in good agreement with values determined experimentally at low frequency.[19,34] The values determined in this study for m_e*, m_h*, and ϵ_r, $(0.3 \pm 0.1)m_e$, $(0.8 \pm 0.5)m_e$, and 6 ± 2, respectively, agree within error with those determined for the bulk semiconductor at optical frequencies. Due to difficulties associated with preparation of colloidal dispersions of the required size, significant difficulty was encountered in reducing the error on the above quantities. Ultimately, error was most effectively minimized by making many determinations for nanocrystalline electrodes prepared from well-characterized colloidal dispersions possessing average diameters of 4 and 12 nm. This lower size limit also served to ensure all experiments were performed under conditions of weak or moderate confinement. Our current work in this area is directed at extending such measurements to electrodes prepared from colloidal dispersions possessing smaller average diameters, although a more appropriate model will likely be required.

Related work of interest is a series of studies performed by Nozik and co-workers in which the redox properties of confined ZnO nanocrystallite dispersions were studied.[35] In particular, these workers used pulse radiolysis techniques to produce transient reducing agents in solution. Electron injection efficiency was correlated with the redox couple potential and the potential energy of the conduction band edge determined. We note also a study by Hasse *et al.*, in which the onset of absorption by ZnO was measured as a function of average nanocrystallite diameter.[36] Using bulk values for the effective reduced mass and optical dielectric coefficient of 0.1775 and 3.8, respectively, the observed dependence could be reproduced. These findings are consistent with those determined here of $0.22m_e$ and 6 for the effective reduced mass and optical dielectric coefficient, respectively, and with their observation that bulk values of these quantities are appropriate even for confined nanocrystallites. Finally, we note a study by Hoyer *et al.* in which the confinement energy of electrons in a ZnO electrode constituted from nanocrystallites of different sizes was determined.[1d] The reported findings are consistent with those reported here.

For TiO_2, there do not appear to have been any previous attempts to study the partition of the energy of confinement between the conduction and valence bands. However, there have been numerous studies of the reducing and oxidizing power of photogenerated electron and holes in confined nanocrystallites.[37] We note, in this context, that an implication of our findings is that the reducing power of photogenerated electrons in confined nanocrystallites is not appreciably greater than in bulk TiO_2. Values for effective electron mass determined at optical frequencies vary between $5m_e$ and $100m_e$.[12,31] No value for the effective hole mass had previously been reported, although values less than $1m_e$ had been suggested.[12] The optical dielectric coefficient is estimated as 9 from the visible refractive index. The values determined in this study for m_e*, m_h*, and ϵ_r are $(>10)m_e$, $(0.8 \pm 0.2)m_e$, and 12 ± 4, respectively. As for ZnO, error was most effectively minimized by making many determinations for nanocrystalline electrodes constituted from nanocrystallites possessing average diameters of 2 and 8 nm. Our current work in this area is directed at extending such measurements to electrodes prepared from colloidal dispersions possessing smaller average diameters. As above, a more appropriate treatment of the resulting data will be required.

IV. Carrier Mobilities in Nanocrystalline Semiconductor Films. Determination of the effective electron and hole masses for a nanocrystalline TiO_2 (anatase) film should facilitate elucidation of the mechanism of carrier transport in devices based on such films, for example, the Graetzel cell.[3] Specifically, using the values determined above for m_e*, m_h*, and ϵ_r, the corresponding mobilities (μ) may be calculated using an expression developed by Frohlich and co-workers; see eq 21.[38]

$$\mu = B[\exp(\theta/T) - 1] \tag{21}$$

However, we do note that the resulting mobilities, and the subsequently calculated diffusion coefficients, are approximate as a result of the errors in the values for m_e*, m_h*, and ϵ_r used in the above calculations. θ is the Debye temperature, B is a coefficient given by eq 22, and ϵ_s is the static dielectric

$$B = \frac{1}{(m_e^*)^{3/2}} \frac{h^2}{e} \frac{3^{1/2}}{2\pi^{5/2}} \frac{\epsilon_0 \epsilon_s \epsilon_r}{\epsilon_s - \epsilon_r} \frac{1}{(k\theta)^{1/2}} \tag{22}$$

coefficient. Using an average value of 114 for ϵ_s, a value of 670 K for θ, and the values determined above for m_e* and ϵ_r, we calculate a value of 0.4×10^{-4} m^2 V^{-1} s^{-1} for the mobility of the conduction band electron at 300 K. This is in excellent agreement with values previously reported for this quantity.[39,40] Further, the diffusion coefficient (D) may be calculated using eq 23 and yields a value of 1×10^{-6} m^2 s^{-1}, also in excellent

$$D = \mu kT/e \tag{23}$$

agreement with previously reported values.[40] Adopting a similar approach, it is possible to calculate, for the first time, a value for the hole mobility in TiO_2 (anatase). Specifically, values of 1.6×10^{-3} m^2 V^{-1} s^{-1} and 4×10^{-5} m^2 s^{-1} are obtained for the hole mobility and diffusion coefficient, respectively. We note that the value reported above for the hole mobility in nanocrystalline TiO_2 (anatase) is in excellent agreement with that recently reported by Lantz and Corn for the hole mobility in TiO_2 (rutile).[41] Specifically, these workers have reported a value of 1.6×10^{-3} m^2 V^{-1} s^{-1} for this quantity, although, for the reasons given above, the exact agreement of these two values is likely fortuitious.

It is interesting to calculate the time required for a carrier to transit from the interior of a crystallite to the surface using eq 24. For an electron in an 8 nm diameter particle the transit

$$\tau = R^2/\pi^2 D \tag{24}$$

time is about 2 ps. The corresponding transit time for a hole is about 400 fs. Employing these values in a model which incorporates the appropriate trapping and detrapping processes should facilitate an understanding of charge transport in

nanocrystalline TiO_2 electrodes. Work directed toward this end is currently in progress.

Finally, we note that the above values have been calculated following detemination of the conduction band edge potential of confined amorphous and bulk anatase nanocrystalline electrodes. In extending these studies, this aspect of the method described will be studied by comparing the results of similar experiments on confined amorphous and bulk rutile nanocrystalline electrodes.

Conclusions

Spectroelectrochemical techniques have been used to determine the absolute energy of the valence and conduction band edges of a transparent nanocrystalline ZnO (wurtzite) and TiO_2 (anatase) electrodes. These electrodes were prepared from nanocrystallites possessing average radii close to, and substantially larger than, the radius of a bound exciton in the corresponding bulk semiconductor. Knowing the absolute energies of band edges, the observed increase in band gap energy for electrodes constituted from confined nanocrystallites may be partitioned between the conduction and valence bands. A subsequent treatment of these data permits determination of the effective electron and hole mass within the constituent nanocrystallites of the electrode. The values determined are in agreement, where available, with those previously reported for the bulk semiconductor. Notably, it has proved possible to determine, for the first time, a value for the effective hole mass in TiO_2 (anatase) of $(0.8 \pm 0.2)m_e$. Using this latter value, and the effective mass determined for the electron, mobilities and diffusion coefficients for each of these carriers in a nanoporous−nanocrystalline semiconductor film have been determined. These values, and others determined in a similar fashion, will facilitate modeling of charge transport within nanocrystalline semiconductor films and devices based on such films.

Acknowledgment. This work was supported by the Commission of the European Communities under the Joule II Programme (Contract JOU2-CT93-0356).

References and Notes

(1) (a) Redmond, G.; O'Keeffe, A.; Burgess, C.; MacHale, C.; Fitzmaurice, D. *J. Phys. Chem.* **1993**, *97*, 11081. (b) Rothenberger, G.; Fitzmaurice, D.; Graetzel, M. *J. Phys. Chem.* **1992**, *96*, 5983. (c) Fitzmaurice, D. *Sol. Energy Mater. Sol. Cells* **1994**, *32*, 289. (d) Hoyer, P.; Eichberger, R.; Weller, H. *Ber. Bunsen-Ges. Phys. Chem.* **1993**, *97*, 630. (e) Hoyer, P.; Weller, H. *Chem. Phys. Lett.* **1994**, *221*, 379. (f) Hotchandani, S.; Bedja, I.; Fessenden, R.; Kamat. P. *Langmuir* **1994**, *10*, 17. (g) Lantz, J.; Baba, R.; Corn, R. *J. Phys. Chem.* **1993**, *97*, 7392.

(2) (a) Lindquist, S.-E.; Finnstrom, B.; Tegner, L. *J. Electrochem. Soc.* **1983**, *130*, 351. (b) Lindquist, S.-E.; Lindgren, A.; Zhu, Y.-N. *J. Electrochem. Soc.* **1985**, *132*, 623. (c) Hagfeldt, A.; Bjorksten, U.; Lindquist, S.-E. *Sol. Energy Mater. Sol. Cells* **1992**, *27*, 293. (d) Sodergren, S.; Hagfeldt, A.; Olsson, J.; Lindquist, S.-E. *J. Phys. Chem.* **1994**, *98*, 5552.

(3) (a) O'Regan, B.; Moser, J.; Anderson, M.; Graetzel, M. *J. Phys. Chem.* **1990**, *94*, 8720. (b) O'Regan, B.; Graetzel, M. *Nature* **1991**, *353*, 737. (c) Nazeeruddin, M. K.; Kay, A.; Rodicio, I.; Humphry-Baker, R.; Muller, E.; Liska, P.; Vlachopulos, N.; Graetzel, M. *J. Am. Chem. Soc.* **1993**, *115*, 6382. (d) Hagfeldt, A.; Didriksson, B.; Palmqvist, T.; Lindstrom, H.; Sodergren, S.; Rensmo, H.; Lindquist, S.-E. *Sol. Energy Mater. Sol. Cells* **1994**, *31*, 481. (e) Redmond, G.; Fitzmaurice, D.; Graetzel, M. *Chem. Mater.* **1994**, *6*, 686. (f) Hagfeldt, A.; Graetzel, M. *Chem. Rev.* **1995**, *95*, 49.

(4) (a) Brus, L. *J. Chem. Phys.* **1984**, *80*, 4403. (b) Brus, L. *J. Phys. Chem.* **1986**, *90*, 2555.

(5) (a) Kavan, L.; O'Regan, B.; Kay, A.; Graetzel, M. *J. Electroanal. Chem.* **1993**, *346*, 291. (b) Kavan, L.; Stoto, T.; Graetzel, M.; Fitzmaurice, D.; Shklover, V. *J. Phys. Chem.* **1993**, *97*, 9493.

(6) Spanhel, L.; Anderson, M. *J. Am. Chem. Soc.* **1991**, *113*, 2826.

(7) Such Nernstian behavior is generally observed for metal oxide semiconductors in aqueous solution.

(8) Blok, L.; de Bruyn, P. L. *J. Colloid Interface Sci.* **1970**, *32*, 533.

(9) (a) Brett, M. J.; Parsons, R. R. *Solid State Commun.* **1985**, *54*, 603. (b) Major, S.; Banerjee, A.; Chopra, K. L. *Thin Solid Films* **1985**, *125*, 179.

(10) Hirschwald, W. In *Current Topics in Materials Science;* Kaldis, E., Ed.; North-Holland: New York, 1981; Vol. VII, Chapter 3.

(11) Flood, R.; Enright, B.; Allen, M.; Barry, S.; Dalton. A.; Doyle, H.; Tynan, D.; Fitzmaurice, D. *Sol. Energy Mater. Sol. Cells*, in press.

(12) Kormann, C.; Bahnemann, D.; Hoffmann, M. *J. Phys. Chem.* **1988**, *92*, 5196.

(13) (a) O'Regan, B.; Graetzel, M.; Fitzmaurice, D. *Chem. Phys. Lett.* **1991**, *183*, 89. (b) O'Regan, B.; Graetzel, M.; Fitzmaurice, D. *J. Phys. Chem.* **1991**, *95*, 10525. (c) Redmond, G.; Fitzmaurice, D. *J. Phys. Chem.* **1993**, *97*, 1426. (d) Enright, B.; Redmond, G.; Fitzmaurice, D. *J. Phys. Chem.* **1994**, *98*, 6195.

(14) Pankove, J. I. *Optical Processes in Semiconductors;* Dover: New York, 1971; p 412.

(15) Bardeen, J.; Blatt, F. J.; Hall, L. H. *Proceedings of the Atlantic City Photoconductivity Conference 1954*; Wiley and Chapman and Hall: New York, 1956; p 146.

(16) Urbach, F. *Phys. Rev.* **1953**, *92*, 1324.

(17) Elliott, R. J.; Gibson, A. F. *An Introduction to Solid State Physics and Its Applications;* Macmillan: London, 1974; p 218.

(18) Hummer, K. *Phys. Status Solidi* **1973**, *56B*, 249.

(19) Dietz, R. E.; Hopfield, J. J.; Thomas, D. G. *J. Appl. Phys.* **1961**, *32*, 2282.

(20) Rossler, U. *Phys. Rev.* **1969**, *184*, 733.

(21) Bloom, S.; Ortenburger, I. *Phys. Status Solidi* **1973**, *58B*, 561.

(22) March, N. H.; Parinello, M. *Collective Effects in Solids and Liquids*; Hilger: Bristol, U.K., 1982.

(23) Elliott, R. J. *Phys. Rev.* **1957**, *108*, 1384.

(24) (a) Rossetti, R.; Hull, R.; Gibson, J.; Brus, L. *J. Phys. Chem.* **1985**, *83*, 1406. (b) Brus, L. *J. Quantum Electron.* **1986**, *22*, 1909.

(25) Flugge, S. *Practical Quantum Mechanics*; Springer: Berlin, 1971; Vol. I, p 155.

(26) Baer, W. *Phys. Rev.* **1967**, *154*, 785.

(27) Yoff, A. D. *Adv. Phys.* **1993**, *42*, 173.

(28) (a) Daude, N.; Gout, C.; Jouanin, C. *Phys. Rev. B* **1977**, *15*, 3229. (b) Burdett, J. *Inorg. Chem.* **1985,** *24*, 2244. (c) Sorantin, P.; Schwarz, K. *Inorg. Chem.* **1992**, *31*, 567.

(29) (a) Arntz, F.; Yacoby, Y. *Phys. Rev. Lett.* **1966**, *17*, 857. (b) Vos, K.; Krusemeyer, H. *Solid State Commun.* **1975**, *15*, 949.

(30) Frova, A.; Boddy, P.; Chen, Y. *Phys. Rev.* **1967**, *157*, 700.

(31) (a) Bickley, R *Chem. Phys. Solids Their Surf.* **1978**, *7*, 118. (b) Stalder, C.; Augustynski, J. *J. Electrochem. Soc.* **1979**, *126*, 2007.

(32) (a) Breckenridge, R.; Hosler, W. *Phys. Rev.* **1953**, *91*, 793. (b) Von Hipple, A.; Kalnajs, J.; Westphal, W. *J. Phys. Chem. Solids* **1962**, *23*, 779.

(33) Grant, F. *Rev. Mod. Phys.* **1959**, *31*, 646.

(34) (a) Hutson, A. *Phys. Rev.* **1957**, *108*, 222. (b) Hutson, A. *J. Appl. Phys.* **1961**, *32*, 2287.

(35) (a) Nozik, A.; Williams, F.; Nenadovic, M.; Rajh, T.; Micic, O. *J. Phys. Chem.* **1985**, *89*, 397. (b) Nedeljkovic, J.; Nenadovic, M.; Micic, O.; Nozik, A. *J. Phys. Chem.* **1986**, *90*, 12.

(36) Haase, M.; Weller, H.; Henglein, A. *J. Phys. Chem.* **1988**, *92*, 482.

(37) Graetzel, M. *Heterogenerous Photoelectrochemical Electron Transfer*; CRC Press: Boca Raton, FL, 1989; Chapter 3.

(38) Fronhlich, H.; Mott, N. *Proc. R. Soc. London* **1939**, *A171*, 496.

(39) Finklea, H. *Semiconductor Electrodes*; Elsevier: New York, 1988; Chapter 2.

(40) Graetzel, M.; Frank, A. *J. Phys. Chem.* **1982**, *86*, 2964.

(41) Lantz, J.; Corn, R. *J. Phys. Chem.* **1994**, *98*, 9387.

JP951142W